TÜBİTAK

Turkish Journal of Earth Sciences

http://journals.tubitak.gov.tr/earth/

Research Article

Turkish J Earth Sci
(2020) 29: 1189-1210

doi:10.3906/yer-2002-18

Assessment of acid mine drainage formation using geochemical and static tests in Mutki (Bitlis, SE Turkey) mineralization area

Mehmet Ali GÜCER*, **Selçuk ALEMDAĞ**, **Enver AKARYALI**

Department of Geological Engineering, Faculty of Engineering and Natural Sciences, Gümüşhane University, Gümüşhane, Turkey

Received: 24.02.2020 • **Accepted/Published Online:** 25.09.2020 • **Final Version:** 16.11.2020

Abstract: In this study, geochemical analyses, as well as short-term contact leaching and acid-base accounting tests, were carried out to determine the occurrence of acid mine drainage (AMD) by static tests in the ore stockpile areas at the Mutki Cu-Fe-Cr deposit (Bitlis, SE Turkey). According to the short-term contact leaching tests, the high enrichment in trace element concentrations in ore-bearing samples, especially in potentially toxic metals such as Cr, Cu, Mn, and Zn, were directly related to sulphide and oxide mineralizations. The pH (3.27–4.05) values of water samples, together with the classification of the intracontinental water resources, indicated that the water quality is the fourth class. Leaching tests, paste pH (3.42–4.46) and sulphide-sulphur (3.9–13.4 wt%) values also suggested that there was AMD production potential in the mineralization area. The AMD production potential was supported by the high mobility of several elements, such as Fe, Mg, Cr, As, Cu, S, and Zn. In ore samples, net neutralization potential (NNP) and net potential ratio (NPR) values were less than –20 kg $CaCO_3$/t and 1, respectively. The basalts forming the basement rock of the stockpile area were characterized by permeable to slightly permeable properties that potentially increase the contamination risk of the groundwater due to seepage in the stockpile area. In order to prevent seepage in the stock area, geomembrane (synthetic waterproofing covers) should be laid at the base to ensure impermeability. The improvements planned in the stock area were modeled by the finite element method and seepage discharges at a depth of 5 m were determined as $1.34 \times 10^{-17} m^3/s$. Thanks to these planned applications, surface and groundwater pollution can be efficiently prevented.

Key words: Acid mine drainage, acid base accounting, contact leaching, finite element groundwater seepage, geomembrane

1. Introduction

The primary source of water and soil pollution in mining activity is acid mine drainage (AMD), mostly occurring in sulphide, coal, and asphaltite mines (e.g., Singer and Stumm, 1970; Brady et al., 2000; Skousen et al., 2000a; Lapakko, 2002; Siddharth et al., 2002; Şanlıyüksel Yücel and Baba, 2013, 2016; Dold, 2014; Şanlıyüksel Yücel et al., 2016; Tosun, 2017; Balcı and Demirel, 2018). The AMD is triggered by the reaction of sulphide minerals (such as pyrite, chalcopyrite, galena, sphalerite, and pyrrhotite) with air (oxygen) and water under atmospheric conditions, often with the contribution of microorganisms e.g., Acidophilic bacterium, Acidithiobacillus ferrooxidans (Singer and Stumm, 1970; Sobek et al., 1978; BCAMDTF, 1989; EPA, 1994a,b; Skousen et al., 2000b; Price, 2003; MEND, 2009; Lottermoser, 2010; Dold, 2014, 2017; Betrie et al., 2015; Liu et al., 2017; Jia et al., 2018; Çimen et al., 2018). When the sulfur-bearing minerals react with oxygen and water during the mining activities or after the mining operation, several potentially toxic metals (Fe, Pb, Cu, Zn, etc.) dissolve and transport with drainage water (Skousen et al., 2000b; Morin and Hutt, 2001; Akçil and Koldaş, 2006; Lottermoser, 2010; De Capitani et al., 2014; Dold, 2017; Akaryalı et al., 2018; Khoeurn et al., 2019). AMD can occur naturally without any human intervention, but it can be significantly enhanced by anthropogenic activities such as mining operations. Several ore-deposit types are commonly associated with AMD including volcanogenic massive sulphide, high-sulfidation epithermal deposits, porphyry copper, and skarn deposits. In recent years, a number of studies have been carried out on the kinetics of pyrite oxidation in both abiotic and biotic systems (e.g., Singer and Stumm, 1970; Boon and Heijnen, 1998; Holmes and Crundwell, 2000; Descostes et al., 2004; Bouffard et al., 2006; Gleisner et al., 2006; Brunner et al., 2008; Nordstrom, 2009; Lottermoser, 2010; Ma and Lin, 2013; Bouzahzah et al., 2014; Dold, 2017; Liu et al., 2017; Michaud et al., 2017; Jia et al., 2018).

In previous studies, investigators generally focused on AMD processes and on the understanding of their potential environmental consequences (e.g., Singer and Stumm, 1970; Lawrence et al., 1989; Blowes and Jambor, 1990;

* Correspondence: maligucer@gmail.com

Gray, 1997; Price, 2003; Dold et al., 2009; Cidu and Frau, 2009; Şanlıyüksel Yücel and Baba, 2013, 2016; Parbhakar-Fox et al., 2013; Dold, 2014; Kalyoncu Erguler et al., 2014; Yolcubal et al., 2016, 2017; Balcı and Demirel, 2018; Park et al., 2019; Kalyoncu Erguler and Erguler, 2020). In the study of Balcı and Demirel (2018) on the prediction of AMD in Küre copper mine, they showed that high Fe, Cu, Zn, Ni, Pb, Cd, Co, and As concentrations were caused by pyrite-rich wastes. In addition, the researchers concluded that the main source of AMD and metal contamination in the region is ore-rich wastes. Similarly, Şanlıyüksel Yücel and Baba (2016) determined that pyrite oxidation, which is commonly found in coals and mine wastes, was the main factor controlling AMD production in Etili coal mine. Also, they concluded that the lack of carbonate rocks in the mine site had an impact on the development of AMD.

Additionally, it is previously stated that the kinetic column and humidity cell tests are commonly used for predicting the potential for AMD formation, and represented actual field conditions better than static tests (e.g., Bradham and Caruccio, 1991; Lawrence and Marchant,1991; Sapsford et al., 2009; Parbhakar-Fox et al., 2013; Kalyoncu Erguler et al., 2014, and references therein). Also, in a current study conducted by Kalyoncu Erguler and Erguler (2020), it was revealed by many statistical evaluations that the key parameters controlling the acid production rate were a time of duration and pH of drainage water.

In this study, the short-term acid production potential of ore samples was investigated by using mineralogical, geochemical, and static tests. With the difference from a large number of studies in the literature, geomembrane was applied to make the stockpile base impermeable in order to prevent groundwater pollution. Another focus of the current study is to model the stock area with finite element-based seepage analysis. In this way, the control of the improvement was made by determining the leakage discharges at a depth of 5 m from the surface numerically. As a result of these studies, in addition to evaluating the potential AMD hazard, possible groundwater pollution will be prevented.

2. Description of the study area

2.1. Hydrology and meteorological conditions

The open pit mine (ore deposit) is located within the drainage area of the surface waters. Gümüşkanat Stream flows approximately 150 m north of the area where the ore material extracted from the mine area will be stored. According to BH-135 drilling cores in the stock area and the surrounding rocks, the basement rock consists of articulated basalt and does not show aquifer characteristic.

The weather conditions of Bitlis can be harsh with long winters and heavy snowfalls. It has a dry-summer continental climate according to the Köppen climate classification (Köppen, 1918). The annual precipitation rate and monthly average precipitation for the summer period in the study area is 1201 mm and 30 mm, respectively. Moreover, the daily mean temperature of the region is 9.5 °C, and the average temperature in April and May are 7.6 °C and 13.2 °C, respectively.

2.2. Geological setting and mine characteristics

The Mutki (Bitlis) mineralization area is located in eastern Turkey which is known as a geologically complex domain of tectonic units which is a part of the Alpine-Himalayan orogenic belt (Şengör et al., 2003; Keskin et al., 2006; Figure 1a and 1b). In the region, there are numerous and different types of mineral deposits ranging from Cambrian to Quaternary (e.g., İmer et al., 2014, 2016, and references therein). Moreover, ophiolites and metamorphic rocks crop out in the studied area (Figure 1c). The rocks in the deposit area comprise two main units: (i) the Mutki Group and (ii) the Guleman Ophiolites. The mineralization area is located in the limestone and ophiolitic rocks (Figure 1c). In the ore deposit field, host rocks generally consist of gabbro, diabase, basic dykes and volcanic rocks, limestone and subordinately schists, and metabasalts. According to BH-135 drilling cores in the stock area and the surrounding rocks, the basement rock consists of articulated basalt and does not show aquifer characteristics.

The Mutki Cu-Fe-Cr mine has been exploited by open pit and underground mining methods. The main ore occurs in the diabasic and gabbroic rocks and is related to NW-SE extending fracture zones. Ore mineral assemblages consist of chalcopyrite, hematite, magnetite, pyrite, bornite, galena, and sphalerite; gangue minerals are mainly represented by quartz and calcite. Hematitic-, limonitic- (Figure 2a), siliceous-, and argillic-crusts, as well as malachite and azurrite precipitates (Figure 2c), are commonly present around the main mineralized zones. The gossans, cropping out at the surface of mineralized zones, range in thickness from 0.25 to 1 m (Figures 2a and 2b), and are easily recognized by their yellow-brown color. The mine is still active, the grade of the exploited Cu mineralization varies between 1.05%–1.50% and the total estimated reserve is 7.211.376 tons. The mine area has a storage location in the northwest of the ore deposit (Figure 3).

3. Materials and methods

3.1. Sampling

In the study area (38°16’7.02” N; 41°41’54.09” E), ten samples from hematite, magnetite, and pyrite bearing mineralizations and ten samples from host rocks including basalts, gabbro, and serpentinite were collected by applying a systematic sampling (Figure 3). The ore-bearing rocks

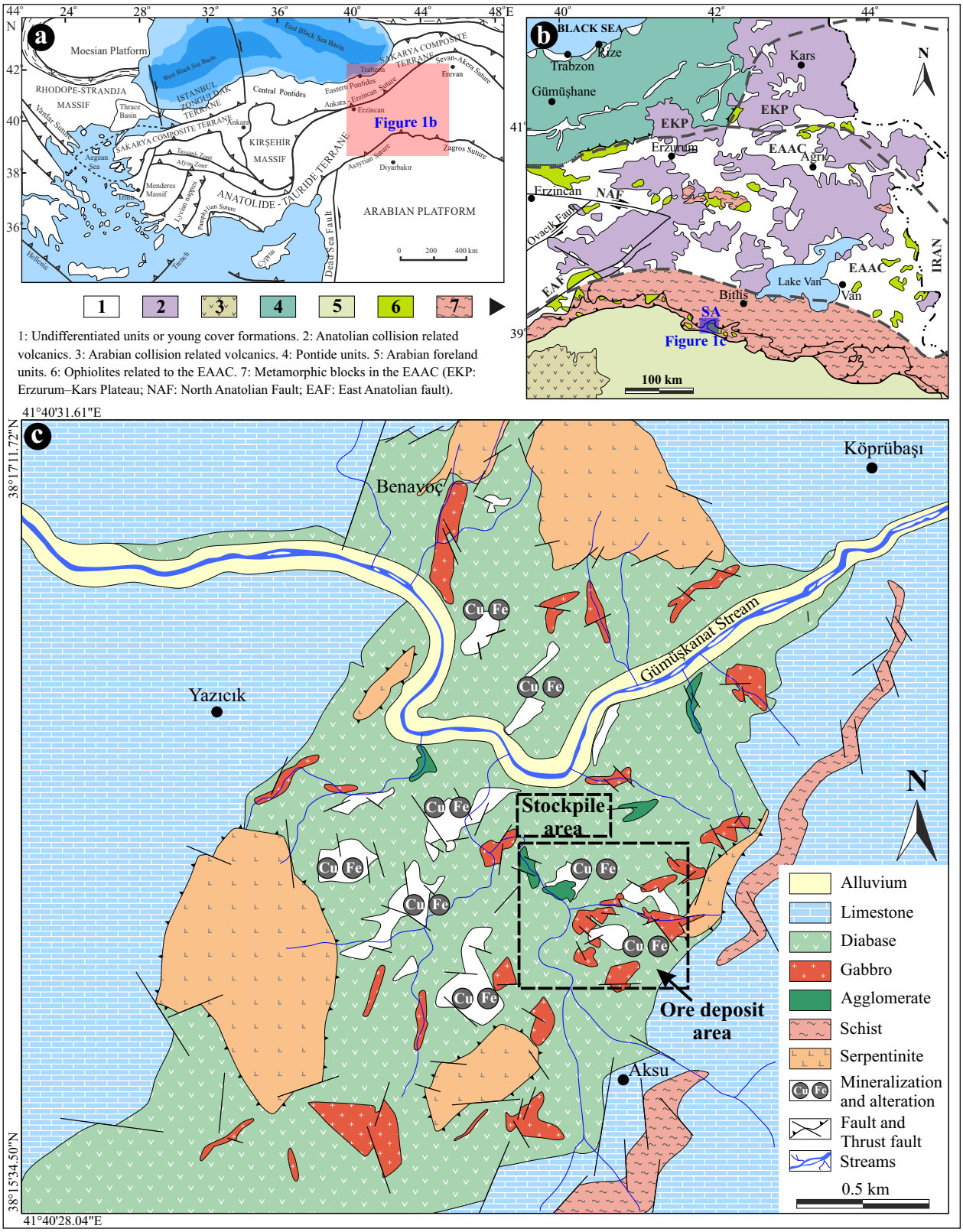

Figure 1. **(a)** Map of the main tectonic units of Turkey (modified after Okay and Tüysüz, 1999). **(b)** Simplified geological map of Eastern Turkey (modified from Şengör et al., 2003; Keskin et al., 2006; Karsli et al., 2008) and location of the study area (SA). **(c)** Simplified geological map of the study area.

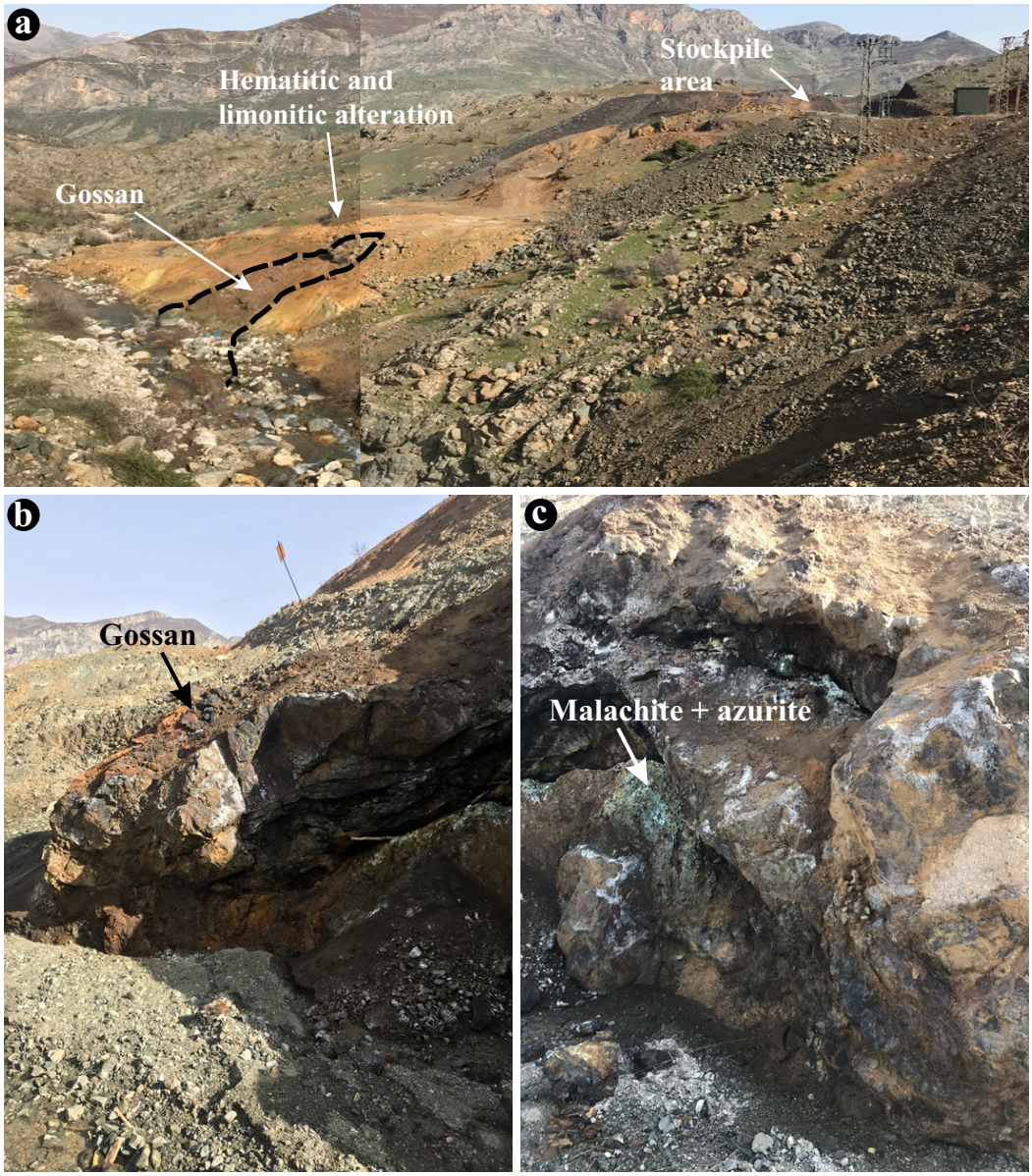

Figure 2. Field photographs of ore and host rocks from the study area. **(a)** Gossan, hematitic and limonitic alteration. **(b)** The view of gossan. **(c)** Malachite and azurite.

were sampled both in the ore deposit and stockpile areas (Figure 3). At the same time, in order to determine the rock mass permeability properties of the stockpile area, samples obtained from the drilling in the study area were compiled and laboratory experiments were conducted. Then, discontinuity properties were determined using the scan-line survey method to determine the rock mass classification in field studies (ISRM, 2007).

3.2. Whole-rock geochemical analysis

Whole-rock chemical analyses were carried out at SGS Analytical Laboratories, Dilovası, Kocaeli (Turkey). Major oxides were analyzed by inductively coupled plasma atomic emission spectrometry (ICP-AES), and trace element compositions were determined by inductively coupled plasma optical emission spectrometry (ICP-OES). Besides, metals such as Ag and Zn were determined with atomic absorption spectrometry (AAS). Samples were crushed into small chips of 0.1–1 cm using a jaw crusher and then powdered using a mild-steel mill. For major elements, samples were prepared with 0.2 g of rock powder fused with 1.5 g $LiBO_2$. Loss on ignition (LOI) was defined as the difference in weight before and after ignition at 1000°C. The detection limits were approximately 0.01 to 0.1 wt% for major oxides and 0.1 to 10 ppm for trace elements.

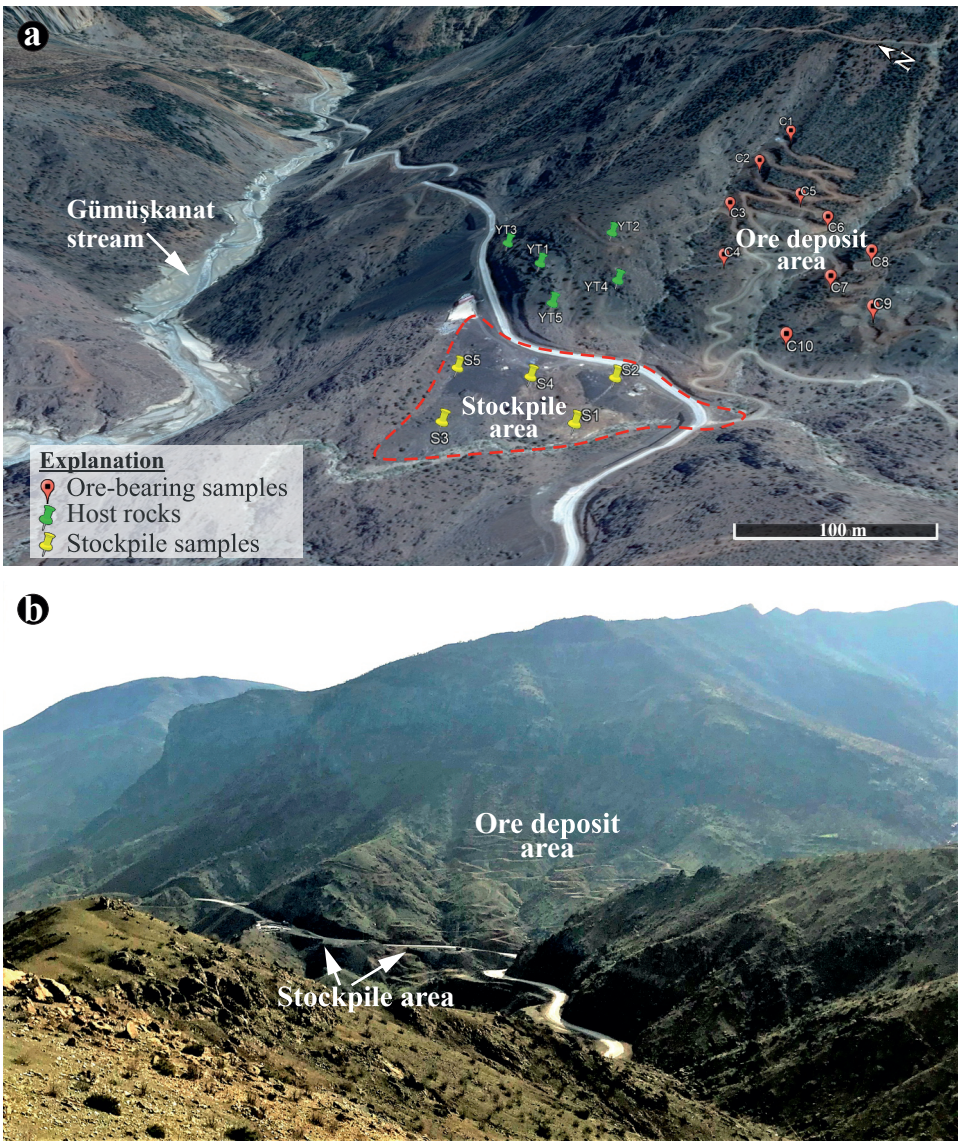

Figure 3. (a) Satellite view of the study area (38° 16' 7.02" N; 41° 41' 54.09" E) with the location of the sampling points: i) red-square pin: ore samples; ii) green-pushpin: host rock samples; iii) yellow-pushpin: ore stockpile samples. Modified from GoogleEarth® image; **(b)** Panoramic photograph showing ore deposit and stockpile areas.

3.3. Leaching tests

Contact leachate tests were carried out at Gümüşhane University, Laboratory of the Department of Food Engineering of the Faculty of Engineering and Natural Sciences (Turkey). The analyses were performed according to the the United States Environmental Protection Agency standard (modified US EPA 1312). The samples were subjected to contact leachate tests with deionized water for 24 h with a 3:1 liquid/solid ratio. In addition, in order to prevent precipitation during the analysis, 2% HNO_3 solution was prepared from Nitric acid (HNO_3) 65% Suprapur, and one drop was added to the water samples. Trace element concentrations were determined with Agilent 7700 inductively coupled plasma-mass spectrometer (ICP-MS).

3.4. Acid-base accounting (ABA) tests

The ABA tests for the characterization of AMD were performed in Düzen Norwest A.Ş. (Ankara, Turkey) environmental laboratory. These tests help determine the tendency of the waste rocks, tailings, and/or sulfur-bearing ore rocks to generate acid drainage. Besides, the concentrations of carbonate and neutralization potential (NP) were determined in all samples. Paste pH analysis was carried out according to the Canadian Mine Environment

Neutral Drainage (MEND, 2009) standard. Moreover, MEND Project 1.20.1 (MEND, 2009) standards were used for NP, acid production potential (AP), and NNP analyses. In addition, total sulphur (%), acid leachable SO_4-S (%), sulphide (%), total carbon (%), and carbonate (%) analyses were performed according to the "ASTM E1915-07A" standard. NP and AP values were calculated from [50 ′ (N of HCl ′ total HCl added-N NaOH ′ NaOH added)] and [% Sulphide-Sulphur ′ 31.25 (Sobek et al., 1978)] formulas, respectively. The most used method to estimate AP is based on the sulfur content and it is calculated by multiplying the sulphide-S content (wt%) by a factor of 31.25 (Sobek et al., 1978; Lawrence and Wang, 1996; Lawrence and Scheske, 1997; Frostad et al., 2003).

3.5. Engineering applications and experiments

In order to calculate the permeability of the rock mass in the stockpile area, samples of the cores obtained from the BH-135 borehole opened in the study area were examined and rock quality designation (RQD) value was determined using the empirical equation (Eq. 1) proposed by Deere (1964).

$$RQD = \frac{\sum Length\ of\ Core\ Pieces > 10cm\ (4in)}{Total\ Core\ Run\ Length} \times 100\% \quad (1)$$

The material properties of the basalts used in the numerical analyses were obtained from laboratory experiments (modulus of elasticity, uniaxial compressive strength, unit weight) carried out in the core samples obtained from BH-135. Laboratory tests were carried out according to the methods proposed by the International Society for Rock Mechanics (ISRM) (2007).

The properties of the rock mass and material (Table 1) based on the in-situ and laboratory data were used to determine the seepage within the rock mass in the stockpile.

In order to determine the permeability of the rock mass, generalized Hoek–Brown criterion (Hoek et al., 2002) was used as the failure criterion in the RS2 numerical analysis method. The parameters mb, s, and a given in Table 1 for the numerical analysis method are the rock mass constants of the basalts in the stock area. Geological strength index (GSI), intact rock constant (mi), and disturbance factor (D) parameters were used accordingly. The properties of the geomembrane to be laid on the base to ensure impermeability in the stock area are given below. Accordingly, the minimum thickness for geomembrane properties: 1.425 mm; breaking stress: 40 kN/m; tear resistance: 187 N; liquid impermeability; $<1\times10^{-6}$ $m^3/(m^2$ day) were used.

4. Results and discussion

4.1. Geochemistry of ore-bearing samples and host rocks

Representative whole-rock major and trace element analyses of the samples from the study area are summarized in Tables 2–3 and Figure 4.

Loss on ignition (LOI) values of the samples is generally high (2.58–34.20 wt%) depending on hydrothermal alteration in the deposit area. The major element contents of the ore samples generally have values close to or below the average composition of basaltic rocks (ACB: Yaroshevsky, 2006; Figure 4a). However, Fe_2O_3, MgO, and Cr_2O_3 contents were higher than the average composition

Table 1. The parameters used in numerical analysis and geomembrane properties.

Material Properties	Basalt	Material Properties	HDPE Geomembran
Unit weight (MN/m^3)	0.02697	Unit weight (kN/m^3)	11.77
Elastic type	isotropic	Thickness (mm)	2.0
Young's modulus (MPa)	7156.8	K (m/s)	4.63e-11
Poisson's ratio	0.25	Tear strength (kN/m)	125
Failure Criterion	Generalized Hoek-Brown	Tensile strength (MPa)	26
Material type	Plastic	Low temperature behavior	Up to -30°
Compressive strength (MPa)	95		
m_b	3.5064	*HDPE (high density polyethylene)	
s	0.002218	*K (Hydraulic conductivity)	
a	0.508086		
Hydraulic model	Simple		
K (m/s)	1.7e-05		
K_2/K_1	1		

Table 2. Major oxide composition (wt%) of representative ore-bearing samples and host rocks from the mineralization area.

Major oxide	SiO_2	Al_2O_3	TiO_2	Fe_2O_3	MgO	MnO	CaO	Na_2O	K_2O	P_2O_5	LOI*	Total
Detection limit	0.01	0.01	0.01	0.01	0.01	0.01	0.01	0.01	0.01	0.01		
ACB**	50.20	14.97	1.40	8.82	7.54	0.18	11.73	2.41	0.19	0.14		
Sample	Ore-bearing samples											
C1	35.20	4.93	0.19	**29.50**	**12.50**	0.12	4.74	0.43	UDL	UDL	9.48	96.98
C2	33.20	4.16	0.15	**34.30**	**10.90**	0.10	4.65	0.32	UDL	UDL	7.76	95.43
C3	32.50	4.15	0.14	**38.60**	**10.00**	0.09	4.65	0.37	UDL	UDL	11.20	101.63
C4	32.00	3.20	0.12	**42.50**	**10.70**	0.12	4.65	0.36	UDL	UDL	3.96	97.58
C5	31.60	3.21	0.13	**35.50**	**10.50**	0.10	5.18	0.38	0.02	UDL	8.86	95.55
C6	18.70	1.79	0.11	**62.40**	4.98	0.07	2.56	0.12	UDL	UDL	6.59	97.35
C7	36.10	5.50	0.22	**33.60**	**14.50**	0.14	5.06	0.20	UDL	UDL	8.37	103.74
C8	36.40	4.46	0.19	**27.40**	**12.30**	0.11	4.51	0.28	0.14	UDL	9.57	95.41
C9	37.00	3.91	0.24	**34.30**	**11.20**	0.11	4.56	0.30	**0.26**	UDL	7.85	99.77
C10	39.20	4.72	0.21	**30.30**	**13.20**	0.13	5.46	0.34	**0.33**	UDL	8.95	102.96
Minimum	18.70	1.79	0.11	27.40	4.98	0.07	2.56	0.12	0.02			
Maximum	39.20	5.50	0.24	62.40	14.50	0.14	5.46	0.43	0.33			
Average	33.19	4.00	0.17	36.84	11.08	0.11	4.60	0.31	0.19			
Sample	Host rocks											
S1	48.90	**15.20**	**2.80**	**14.00**	4.10	**0.25**	6.85	**3.85**	**2.55**	**1.55**	<0.01	99.90
S2	17.70	0.95	0.05	1.04	4.31	0.04	**39.60**	0.07	0.44	0.01	34.20	98.46
S3	47.30	14.80	**2.84**	**13.20**	3.57	**0.23**	6.99	**3.67**	**2.50**	**1.49**	<0.01	96.63
S4	50.40	14.10	**2.77**	**13.00**	3.89	**0.23**	6.48	**3.57**	**2.29**	**1.42**	<0.01	97.58
S5	43.10	4.78	0.13	**9.16**	**30.00**	0.14	4.64	0.15	0.20	UDL	6.77	102.91
YT1	**54.40**	14.80	0.99	**12.50**	5.85	0.13	5.53	**2.98**	**1.22**	0.04	3.39	101.79
YT2	**55.40**	14.70	0.34	**9.03**	7.42	0.16	6.78	**2.44**	**1.10**	0.01	4.08	101.50
YT3	**53.30**	14.00	0.80	**11.70**	6.04	0.13	5.20	**3.11**	**1.06**	0.03	2.58	97.90
YT4	**55.50**	14.30	0.73	**11.20**	6.51	0.13	5.78	**3.10**	**1.13**	0.04	2.99	101.34
YT5	**55.90**	14.70	0.78	**11.00**	6.03	0.13	5.68	**3.08**	**1.01**	0.04	3.28	101.73
Minimum	17.7	0.95	0.05	1.04	3.57	0.04	4.64	0.07	0.2	0.01		
Maximum	55.9	15.2	2.84	14	30	0.25	39.6	3.85	2.55	1.55		
Average	48.19	12.23	1.22	10.58	7.77	0.16	9.35	2.60	1.35	0.51		

*LOI: Loss on ignition, **ACB: Average composition of basaltic rocks (Yaroshevsky, 2006). UDL: Under detection limit. Values above average are shown in bold.

in relation to the basic rocks (e.g. ophiolites) in the study area. The contents of the SiO_2 and Al_2O_3 in the rocks have a wide range (from 18.70 to 39.20 wt% and from 1.79 to 5.50 wt%, respectively). Additionally, they have low Na_2O content (up to 0.43 wt%). Moreover, MnO and CaO vary between 0.07–0.14 wt% and 2.56–5.46 wt%, respectively. The Fe_2O_3 enrichment in ore samples could be related to the chemical composition of the ore minerals such as hematite, magnetite, pyrite, and chalcopyrite. Similarly, high CaO content is related to the carbonate host rocks (limestone, dolomite, marl, etc.), which contain mineralizations.

In the host rocks, SiO_2, Al_2O_3, and CaO contents ranged between 17.70–55.90 wt%, 0.95–15.20 wt% and 4.64–39.60 wt%, respectively. In addition, Fe_2O_3 and MgO contents vary from 1.04–14.00 wt% and 3.57–30.0 wt%. The wide range of major oxide contents in the samples is associated with the different host rock types such as limestone, diabase, gabbro, agglomerate, serpentinite, and schist. Generally, there are increases in SiO_2, Al_2O_3, TiO_2, Fe_2O_3, MgO, Na_2O, and K_2O contents in comparison with the ACB for studied samples (Table 2). According to compared ACB (Yaroshevsky, 2006), the high Fe_2O_3

Table 3. Trace element composition (ppm) of representative ore-bearing samples and host rocks from the mineralization area.

Trace element	Ag	As	Ba	Bi	Cd	Cr	Cu	Hg	S (wt%)	Sb	Sr	Zn	Zr
Detection limit	2	3	10	5	1	1	0.5	1	0.01	5	20	10	10
ACB*	0.1	2	300	0.007	0.19	200	100	0.09	0.03	1	440	130	100
Sample	Ore-bearing samples												
C1	**7**	**106**	24	UDL	**1**	**684**	**>10000**	UDL	**5.87**	**9**	UDL	**588**	17
C2	**3**	**51**	17	UDL	UDL	**616**	**>10000**	UDL	**6.36**	**6**	UDL	**211**	13
C3	**2**	UDL	UDL	UDL	UDL	**684**	**>10000**	UDL	**9.82**	UDL	UDL	39	12
C4	UDL	**20**	14	UDL	UDL	**684**	**>10000**	UDL	UDL	**7**	UDL	120	16
C5	**3**	**25**	UDL	UDL	UDL	**821**	**8860**	UDL	**6.7**	**9**	UDL	119	15
C6	UDL	**18**	16	UDL	UDL	**616**	**6159**	**2**	UDL	**8**	UDL	103	15
C7	**4**	**25**	UDL	UDL	UDL	**889**	**>10000**	**1**	**5.98**	**7**	UDL	122	UDL
C8	**3**	**22**	13	UDL	UDL	**616**	**>10000**	UDL	**6.81**	UDL	UDL	92	11
C9	**8**	**41**	14	UDL	UDL	**684**	**>10000**	UDL	UDL	**8**	UDL	93	22
C10	**4**	**34**	13	UDL	UDL	**753**	**5417**	UDL	UDL	**6**	UDL	126	20
Minimum	2	18	13			616	5417		5.87	6		39	11
Maximum	8	106	24			889	10000		9.82	9		588	22
Average	4.25	38.00	15.86			705	6812		6.92	7.50		161.30	15.67
Sample	Host rocks												
S1	UDL	UDL	**549**	UDL	UDL	UDL	50	UDL	**0.07**	UDL	**494**	**308**	**367**
S2	UDL	**23**	27	UDL	UDL	UDL	46	UDL	**0.13**	UDL	**923**	106	15
S3	UDL	UDL	**605**	UDL	UDL	UDL	45	UDL	**0.08**	UDL	**491**	**295**	**369**
S4	UDL	UDL	**484**	UDL	UDL	UDL	27	UDL	0.03	UDL	**463**	105	**344**
S5	UDL	**50**	**350**	UDL	**2**	**2532**	**152**	UDL	**0.17**	**5**	28	**739**	14
YT1	UDL	UDL	18	UDL	UDL	UDL	15	UDL	0.01	UDL	168	UDL	43
YT2	UDL	UDL	UDL	UDL	UDL	UDL	15	UDL	UDL	UDL	135	UDL	41
YT3	UDL	UDL	21	UDL	UDL	UDL	33	UDL	UDL	UDL	161	10	47
YT4	UDL	**3**	19	UDL	UDL	UDL	31	UDL	0.01	UDL	165	UDL	49
YT5	UDL	**3**	18	UDL	UDL	UDL	11	UDL	UDL	UDL	160	UDL	45
Minimum		3	18				11		0.01		28	10	14
Maximum		50	605				152		0.13		923	739	369
Average		19.75	232				43		0.071		319	261	133

*LOI: Loss on ignition, **ACB: Average composition of basaltic rocks (Yaroshevsky, 2006). UDL: Under detection limit. Values above average are shown in bold.

values in the host rocks are related to the abundant mafic minerals such as pyroxene, amphibole, and biotite, but the high values may also indicate that minerals are subjected to hematitic and limonitic alteration.

The trace element distributions of both host rocks and especially ore samples exhibit a higher enrichment compared to the average continental crust composition (Table 3). In the ore deposit area, there were high enrichments in Cr, Cu, Mn, S, and Zn associated with mineralizations. Extremely high concentrations are found for Cu ((from 5417 to >10000 ppm) and Cr (616–890 ppm). Other elements in ore-samples with high concentrations include S and Zn, varying from 58700–98200 ppm and 39–588 ppm (Figure 4b), respectively, whereas in the host rocks Mn has the highest enrichment ranged between 310 and 1936 ppm (Table 3).

As a result, the various distributions in the elemental concentration indicate different mineralogical compositions. However, high enrichment in trace element concentrations, especially in potentially toxic metals

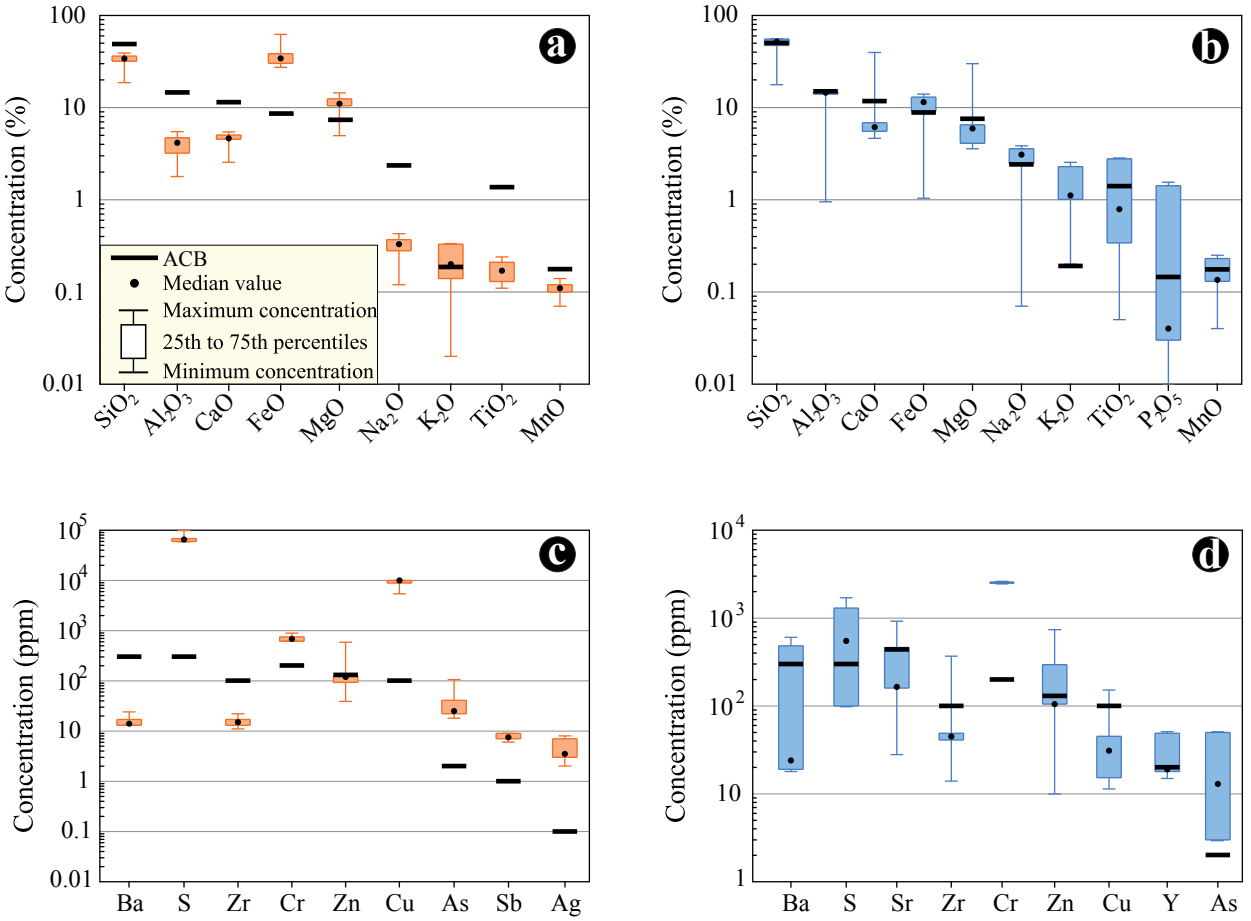

Figure 4. Boxplots presenting summary statistics for selected whole rock major (%) and trace (ppm) element concentration on ore-bearing and host rock samples. **(a)** Ore-bearing samples and **(b)** host rocks of major elements. **(c)** Ore-bearing samples and **(d)** host rocks of trace elements. ACB: Average composition of basaltic rocks (Yaroshevsky, 2006).

such as Cr, Cu, Mn, and Zn is related to chalcopyrite and sphalerite mineralization and/or hydrothermal alteration at the ore deposit area.

4.2. Assessment of water quality

In twenty samples, representative of mineralization (especially in the gossans) and host rocks, short-term contact leaching tests were implemented for the assessment of acid drainage formation and the results are given in Table 4. Also, the samples were compared with quality classification of the intracontinental water resources suggested by RG28483 (2012) and mine drainage waters (Ficklin et al., 1992).

The pH values of leachate from ore samples varied from 3.27 to 4.05 (n = 10), while the host rocks' leachate pH value range was between 5.56 and 6.83 (n = 10). The obtained pH results indicated the acidic environment rather than the alkaline one. When these values were compared with the quality classification of the intracontinental water resources, the pH values of the host rocks leachates indicate the first-class quality, while the values for ore samples represent the fourth class quality waters in terms of pH parameter (Table 4).

Boxplots presenting summary statistics for selected potentially toxic metal concentrations of the samples are presented in Figure 5. The high metal concentrations such as Al, Fe, Cu, Mn, Zn, Cd, Co, Ni, and Pb are found in the lower pH range (3.27–4.05, n = 10), which occur in almost all cases within of the ore-bearing rocks (Figure 5a). The increase in Fe, Cu, Zn, Cd, Co, and Ni concentrations are associated with mineralization such as chalcopyrite, hematite, and magnetite mineralization. Additionally, these increases in concentrations are related to the types of alterations such as hematitic and limonitic, as well as malachite and azurite precipitates observed in the study area. In Figure 5a, Al, and Fe concentrations are distributed over a wide range of values, while Na and Mn concentrations are distributed in a narrow range. All element concentrations except Na and Cr are well above water quality standards.

Table 4. Results of contact leaching tests (mg/L) of the ore-bearing samples and host rocks from mineralization area.

	pH	Na	Al	Cd	Co	Cr	Cu	Fe	Mn	Ni	Pb	Zn
Quality Classification of the Intra-Continental Water Resources according to TS266 (RG28483, 2012)*												
I	6.5-8.5	125	≤0.3	≤0.002	≤0.01	≤0.02	≤0.02	≤0.3	≤0.1	≤0.02	≤0.01	≤0.2
II	6.5-8.5	125	≤0.3	0.005	0.02	0.05	0.05	1	0.5	0.05	0.02	0.5
III	6.0-9.0	250	1	0.007	0.2	0.2	0.2	5	3	0.2	0.05	2
IV	< 6.0 or > 9.0	>250	>1	>0.007	>0.2	>0.2	>0.2	>5	>3	>0.2	>0.05	>2
Sample	Ore-bearing samples											
C1	4.05	10.4	**2.60**	**0.38**	**2.4**	0.01	**21.6**	5.0	**16.7**	**13.1**	**1.63**	**60.4**
C2	3.75	13.4	**61.7**	**0.22**	**8.2**	0.01	**192.0**	**96.0**	**14.6**	**27.6**	**0.77**	**32.6**
C3	3.49	10.6	**30.8**	**0.08**	**5.1**	0.02	**296.0**	**158.0**	**7.00**	**28.2**	**0.22**	**9.10**
C4	3.86	6.1	**2.10**	**0.03**	**2.3**	0.01	**176.0**	3.50	**4.70**	**7.40**	**0.36**	**5.10**
C5	3.43	6.9	**75.7**	**0.13**	**5.2**	0.09	**418.0**	**162.0**	**6.80**	**37.2**	**0.81**	**20.4**
C6	3.82	5.5	**2.40**	**0.11**	**0.8**	0.01	**6.90**	**21.5**	**5.60**	**5.20**	**0.47**	**15.0**
C7	3.61	7.0	**57.7**	**0.17**	**3.0**	0.02	**228.0**	**98.0**	**8.40**	**17.6**	**1.03**	**20.6**
C8	3.56	8.1	**88.8**	**0.21**	**4.0**	0.04	**308.0**	**190.0**	**5.20**	**22.0**	**0.34**	**25.7**
C9	3.75	8.2	**9.30**	**0.11**	**2.8**	0.01	**264.0**	**13.1**	**6.70**	**21.4**	**0.45**	**11.9**
C10	3.27	9.8	**149.4**	**0.29**	**4.6**	0.09	**234.0**	**192.0**	**8.30**	**34.7**	**2.25**	**29.6**
	Host rocks											
S1	5.56	15.5	0.6	**0.01**	0.03	0.01	**0.34**	0.7	0.29	0.01	0.05	0.09
S2	5.85	9.10	0.0	**0.01**	0.01	0.01	0.08	0.02	0.06	0.01	0.01	0.01
S3	6.07	15.7	**2.1**	**0.01**	0.02	0.01	**0.23**	0.5	0.52	0.01	0.01	0.01
S4	6.31	14.3	**9.7**	**0.01**	0.02	0.01	0.09	5.0	0.21	0.07	**0.08**	0.07
S5	6.62	11.2	0.1	**0.01**	0.01	0.01	0.06	0.0	0.06	0.01	0.01	0.01
YT1	6.77	16.2	0.7	**0.01**	0.01	0.01	0.06	0.5	0.11	0.01	0.01	0.01
YT2	6.78	14.5	**1.2**	**0.01**	0.02	0.01	0.08	0.9	0.12	0.01	0.01	0.01
YT3	6.77	17.7	**2.1**	**0.01**	0.03	0.01	0.09	1.8	0.11	0.10	0.03	0.18
YT4	6.70	17.3	**13.7**	**0.01**	0.02	0.01	0.07	**8.0**	0.34	0.13	0.03	0.04
YT5	6.83	13.8	**3.7**	**0.01**	0.01	0.01	0.10	3.2	0.16	0.06	0.02	0.08

*TS266: Regulation on surface water quality management, the Turkish Standards, revision: 30.11.2012, number 28483 (revision: RG-15.4.2015-29327); Values above average are shown in bold.

Similarly, there is a significant enrichment in Fe and Al concentrations in the host rocks and not the other potentially toxic metals (Figures 5b). The increase of Fe contents in both ore samples and host rocks also indicated the effects of gossan as well as hematitic and limonitic crusts by the interaction of sulphide mineralizations with meteoric agents in the study area. Since Cd and Cr concentrations have the same value in all samples, they are not statistically significant (Figure 5b). Also, Na, Cu, Zn, and Cr concentrations are well below water-quality standards, whereas Mn, Cd, Co, and Pb concentrations are above.

The influence of climatological conditions, host rocks, alterations, mine process or mining process facilities on the nature of AMD can be illustrated using Ficklin diagrams (Plumlee et al., 1999). These diagrams, in which the sum of the base metals such as Zn, Cu, Cd, Pb, Co, and Ni is plotted against pH, can be used to interpret variations in mine drainage water chemistry between different deposit types (e.g., Ficklin et al., 1992; Plumlee et al., 1992, 1999). The forementioned base metals were selected rather than more common metals such as Fe, Al, and Mn because the selected base metals have been proved as the most diagnostic in differentiating between different geologic controls.

In the Ficklin discrimination diagrams, the samples collected in host rocks plot at the upper left concentration end of the "near-neutral/low-metal" concentration

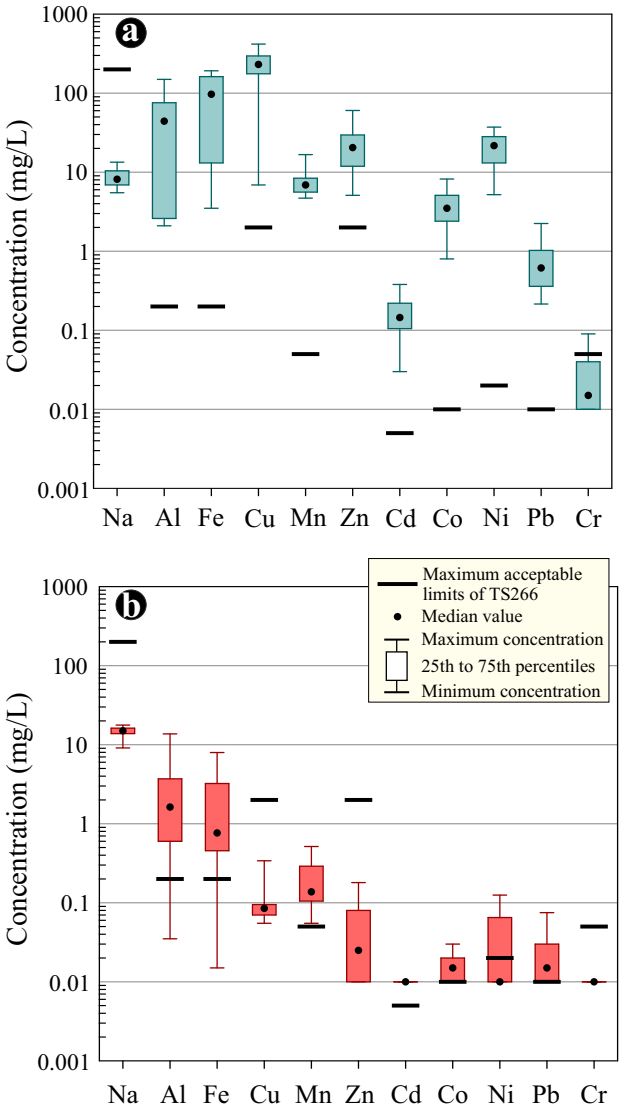

Figure 5. Boxplots presenting summary statistics for selected potentially toxic metal concentrations of filtered and/or acidified water of the **(a)** ore-bearing samples and **(b)** host rocks.

field, while samples collected within ore-bearing rocks predominantly plot in a fairly restricted area at the lower left on the "acid/extreme-metal" concentration fields (Figure 6a). These indicated that the host rocks reflect "neutral mine drainage" features, whereas the ore-bearing samples have potential "acid rock/mine drainage" characteristic, which is supported by the high Cu values of 6.90–418 mg/L. Besides, Ficklin diagrams can be used to describe some principles that manage mine water quality. In the Figure 6b, a number of trend lines display the general effect of pyrite, base-metal sulphide, and carbonate content on mine water quality. As can be seen in the diagram (Figure 6b), an increase in pyrite content tends to result in more acidic, whereas an increase in carbonate content tends to lead to more alkaline waters (e.g. Verburg et al., 2009). Also, an increase in base metal sulphide content tends to result in an increase in trace metal concentrations (Verburg et al., 2009). In Figure 6b, the studied host rocks are typically characterized by 'dilution by surface water' contents. This trend of the host rock samples indicates the greater dilution and reduced solid to water ratio, associated with wetter climates and geological setting (e.g., limestone/dolomite rocks, agglomerate, etc.) of the study area. However, ore-bearing samples tend to increase pyrite content (Figure 6b). This situation is related to the geochemical characteristics of the ore minerals especially pyrite and mine wastes in the study area.

4.3. Assessment of acid-base accounting (ABA)

The ABA is defined simply as the balance between the acid-production and acid-consumption properties of mine waste material (e.g., Smith et al., 1976; Skousen et al., 1987; Hossner and Brandt, 1997; Siddharth et al., 2002). It is used to make static measurements of acid mine drainage potential. Measurements of total sulphur (S%) or sulphide sulphur (S^{2-}%) are used to estimate the amount of acid-bearing material.

ABA static measurement results in the mine and ore stockpile areas are provided in Table 5. Also, the NP, AP, and NNP were determined. In the study field, the ore-bearing samples generally have low paste pH values ranged between 3.42 and 4.46 (n = 10), whereas host rocks exhibit higher pH values varied from 7.76 to 9.93 (n = 10). This fact indicated that the ore-bearing rocks are potential acid-generating materials based on the static test interpretation criteria in Table 6. Recent studies such as the one conducted by Dold (2017) suggested that, for the calculation factor of the sulfide AP for AMD prediction, the 62.5 must be applied when the paste pH is >6.3 because two moles of calcite are needed to neutralize the acidity from one mole of sulfur (assuming pyrite oxidation as the only protons source, and the presence of calcite for neutralizing). Otherwise, if the paste pH is <6.3, the correction factor should be applied as 31.25 for calculation (Dold, 2017). However, in the ore-bearing samples, the sulfur concentrations were multiplied by the factor of 31.25 due to the paste pH values lower than 6.3 (e.g. Dold, 2017).

The AP and NNP contents of the ore-bearing rocks ranged in between 122–419 kg $CaCO_3$/t and from -366 to -63.4 kg $CaCO_3$/t respectively, and the samples fall into the acid-generating zone (n = 10; Figure 7). On the contrary, in the host rocks, AP and NNP ranged from 0.31 to 4.69 (n = 10) kg $CaCO_3$/t and from 10.6 to 865 (n= 10), respectively and samples fall mostly into the non-acid generating zone (Figures 7). This may require a kinetic test on samples with values less than 20 kg $CaCO_3$/t to reveal the potential of acid production. Similarly, the AP and NP values are

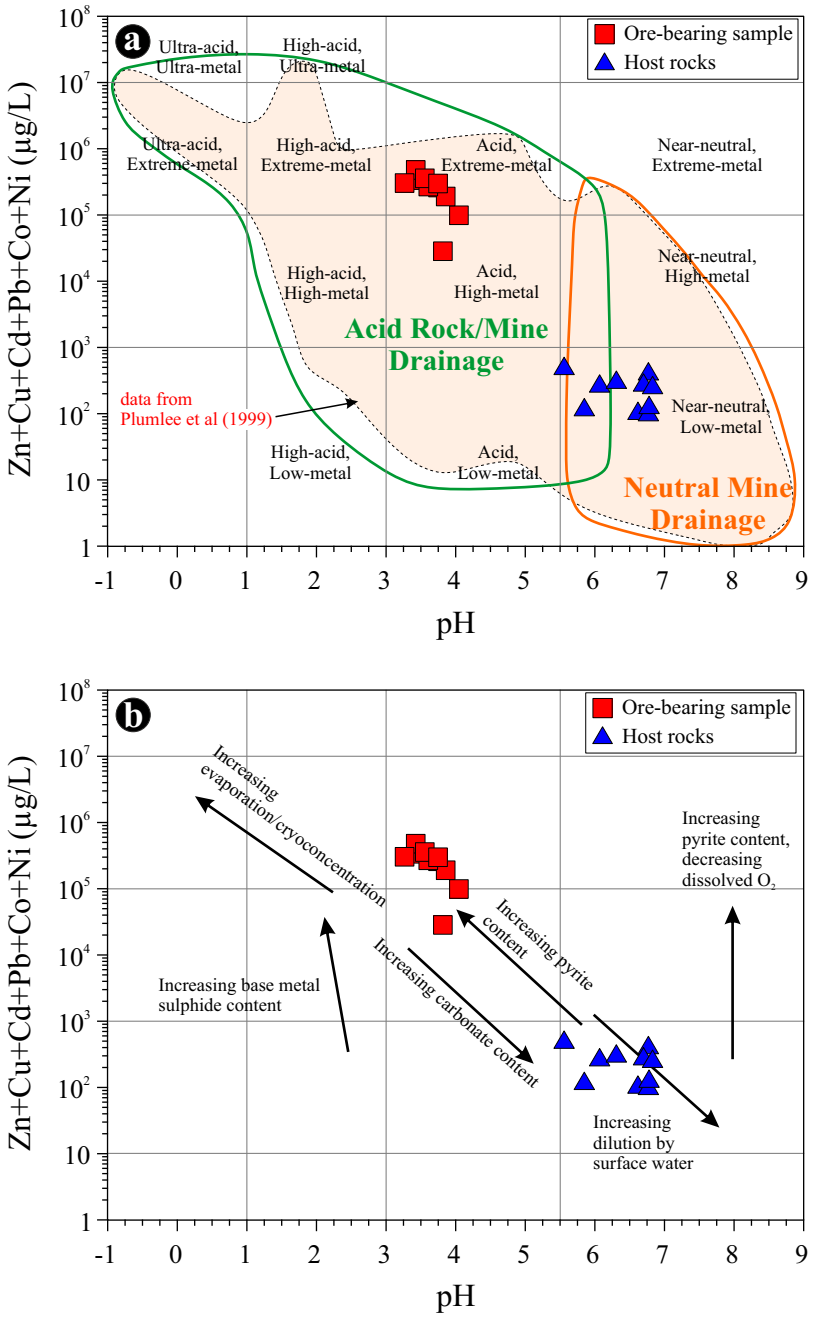

Figure 6. (a) Ficklin geochemical discrimination diagram for the ore-bearing samples and host rocks. **(b)** Trending of the samples in the Ficklin classification plot. The boundaries, names of metal bins and classify different drainage compositions were originally proposed by Ficklin et al. (1992) and Plumlee et al. (1992), data adapted from Plumlee et al. (1999).

proportioned to see whether a sample has a stoichiometric balance that favors net acidity or net alkalinity (e.g., Sobek et al., 1978; Brodie et al., 1991; Price et al., 1997; Soregaroli and Lawrence, 1998; Table 6).

The NPR values in the host rocks varied from 28 to 278 (n = 10) depending on the various rock types. On the contrary, in the ore-bearing samples, the NPR values ranged from 0.13 to 0.48 (n = 10). In case the NPR value is <1, the material is considered to produce acid; whereas, if the value is >3, the material is considered as nonacid producing material (Brodie et al., 1991). According to this fact, host rock samples scattered in the nonacid generating zone, whilst the ore-bearing samples are spotted in the acid-generating zone (Figure 7b, Table 6).

Table 5. Acid base accounting (ABA) analyses of the ore-bearing samples and host rocks from study area.

Sample	Paste pH	NP[1]	AP[2]	NNP[3]	NPR[4]	Sulphur Total S	Acid Leachable Sulfate (SO_4^{2-})	Sulphide S^{2-}	Carbonate $CaCO_3$
Unit	–	kg $CaCO_3$/t	kg $CaCO_3$/t	kg $CaCO_3$/t	-	%	%	%	%
	Ore-bearing samples								
C1	4.46	76.60	219.10	-142.50	0.35	7.000	0.5200	<0.02	2.11
C2	3.89	79.10	256.20	-177.20	0.31	8.200	1.1200	<0.02	2.29
C3	3.59	52.90	418.80	-365.80	0.13	13.400	0.5000	<0.02	2.29
C4	4.38	47.50	121.90	-74.40	0.39	3.900	0.2200	<0.02	2.30
C5	3.60	47.80	300.00	-252.20	0.16	9.600	0.8600	<0.02	2.30
C6	4.19	56.20	162.50	-106.20	0.35	5.200	0.3900	<0.02	2.29
C7	3.78	66.20	265.60	-199.40	0.25	8.500	0.6300	<0.02	2.32
C8	3.72	47.50	309.40	-261.90	0.15	9.900	0.8100	<0.02	2.48
C9	4.11	58.40	121.90	-63.40	0.48	3.900	0.3600	<0.02	2.11
C10	3.42	47.50	156.20	-108.80	0.30	5.000	0.8487	<0.02	2.12
	Host rocks								
S1	7.76	154.70	2.19	152.50	70.64	0.070	0.0030	<0.02	2.67
S2	8.78	868.40	3.12	865.30	278.33	0.100	0.0040	<0.02	78.85
S3	8.11	156.90	2.19	154.70	71.64	0.070	0.0127	<0.02	3.51
S4	8.36	152.20	0.94	151.20	161.91	0.030	0.0013	<0.02	2.49
S5	9.93	153.70	4.69	149.10	32.77	0.150	0.0100	<0.02	2.64
YT1	8.43	59.70	0.31	59.40	192.58	0.010	0.0007	<0.02	2.15
YT2	8.19	61.30	2.19	59.10	27.99	0.070	0.0006	<0.02	2.48
YT3	8.24	67.50	0.31	67.20	217.74	0.010	0.0006	<0.02	2.10
YT4	8.26	65.00	0.31	64.70	209.68	0.010	0.0007	<0.02	2.28
YT5	8.05	10.90	0.31	10.60	35.16	0.010	0.0007	<0.02	2.29

[1]NP (Neutralization Potential) calculated from Sobek et al. (1978) procedure; [2]AP (Acid Production Potential) = % Sulphide-Sulphur x 31.25 (Sobek et al., 1978); [3]NNP (Net Neutralization Potential) = NP – AP; [4]NPR (NP/AP Ratio) = NP/AP; Results expressed as tonnes $CaCO_3$ equivalent/1000 tonnes of material; Samples with a % Sulphide value of <0.02 will be calculated using a 0.02 value.

In polymetallic sulphide mining activities, S^{2-} minerals in ore and host rocks are oxidized by oxygen and water; therefore, the pH of the ground and surface waters decreases (increasing the acidity). The sulphide-sulphur compositions of the ore-bearing samples have a range of 3.90%–13.40%, whereas the compositions of the host rocks range from 0.01% to 0.15%. According to sulphide-sulphur and NPR values, ore-bearing samples potentially reflect acid-generating characteristics (Figure 8). Therefore, acid producing materials have a sulphide-sulphur concentration greater than 0.3%, and they have NPR less than 3:1 ratio (e.g. Sobek et al., 1978). In case of a sulphide-sulphur concentration between 0.1% and 0.3%, the materials are unlikely to be potentially acid-generating in the field (Figure 8).

4.4. Hydraulic conductivity of rock mass in stockpile area

In order to determine the hydraulic conductivity of the rock mass which forms the basis of the stockpile area, samples of the first 50 m depth of BH-135 in the study area were investigated and rock quality designation (RQD) values were determined (Figure 9b).

Since no hydraulic conductivity tests were conducted in the rock mass, the hydraulic conductivity was determined empirically using three different equations depending on the RQD parameter determined in every 1 meter of the drilling cores. The hydraulic conductivity value (K) determined in the equations is (m/s).

$$K = 1950 \times e^{-0.05RQD} \times 10^{8-} \quad (2)$$

$$Lu = -1.52 \times RQD + 153.8 \quad (3)$$

$$Lu\ (RMP) = -8.665 \times \ln(RQD) + 41.229 \quad (4)$$

In the study conducted by Adedokun and Abubakar (2016), 1 Lugeon= 1.3×10^{-7} m/s was used; the same value

Table 6 Static test interpretation parameters

	Screening criterion		
References	**NPR**	**NNP**	**Paste pH**
Price et al. (1997)	<1, Likely AMD potential		pH<4, Acid
	1-2, Possibly AMD potential		pH>7, Neutral
	2-4, Low AMD potential		
	>4, None		
Soregaroli and Lawrence (1998)	<1, Potential acid formation		
	1-3, Inconclusive		
	>4, Has enough neutralizing capacity		
Brodie et al. (1991)	<1, Acid generating		
	1-3, Uncertain		
	>3, None acid generating		
Ferguson and Morin (1991)		<-20, Potential acid formation	
		-20<NNP<20, Uncertain	
		>20, Non-acid formation	
Sobek et al. (1978)		<-5, Acid forming	

The unit of measurement is kg $CaCO_3$ per ton, or equivalently parts per thousand $CaCO_3$

was used in the Lugeon transformation in the current study.

The depth variation of the K permeability coefficient, which is obtained by using the equations proposed by different researchers (Rastegarnia et al., 2019: Eq.2; Farid and Rizwan, 2017: Eq. 3; Kayabasi et al., 2015: Eq. 4), is given in Figure 9a. Accordingly, it was determined that the hydraulic conductivity values decreased from the surface to the deep in the rock mass of the stock area. In addition, statistical values and histograms showing the distribution of hydraulic conductivity values determined from each equation are given in Figures 9c, 9d, and 9e. According to the statistical evaluations, the hydraulic conductivity of the rock mass based on the equations 2, 3, and 4 are 16.87×10^{-8} m/s - 921.11×10^{-8} m/s, 122.2×10^{-8} m/s - 1703×10^{-8} m/s, and 23×10^{-8} m/s-231×10^{-8} m/s, respectively.

According to the obtained hydraulic conductivity, the rock mass was evaluated (ISRM, 1981) and it was determined to be slightly permeable (Table 7). This means that the ore pile to be stored without taking any precautions in the stockpile area can contaminate the groundwater if it creates a possible acid mine drainage form.

4.5. Infiltration modeling of the rock mass in the stock area

Accumulation of sulphide ores obtained from mining areas by open pit method and their exposure to atmospheric conditions without any precautions may cause contamination of groundwater and other severe environmental issues. Many methods have been applied to prevent the formation of AMD (such as laying and compacting clay in the stock area, a drainage trench, neutralization of acid formation by laying limestone on the floor of the stockpile, active and passive purification methods, swamp system, etc). In this study, limestone pebbles were used for the neutralization of AMD (Caraballo et al., 2009, 2011; Delibalta et al., 2016) along with drainage trench in order to prevent surface water from entering the stockpile area. As a second intervention, high density polyethylene (HDPE) geomembrane will be laid to the base of the stockpile area and the floor will thus be almost completely impermeable.

The applications of HDPE geomembrane, clay core, and mechanical compaction in the dam body and waste storage areas were applied by some researchers (Baba et al., 2004; Tayfur et al., 2010; Gurocak and Alemdag, 2012; Alemdag, 2015; Kanık and Ersoy, 2019; Alemdag et al., 2020). With these applications, groundwater and natural environmental pollution will be significantly prevented.

The basement rock of the stock area planned to be constructed consists of basalts and has slightly permeable properties. For this reason, the effect of possible infiltrations on Gümüşkanat Stream is inevitable.

Although basalts spreading in the stock area do not have an aquifer characteristic, joint systems in rock masses will be effective in mixing water with high acidity to be collected in the storage area.

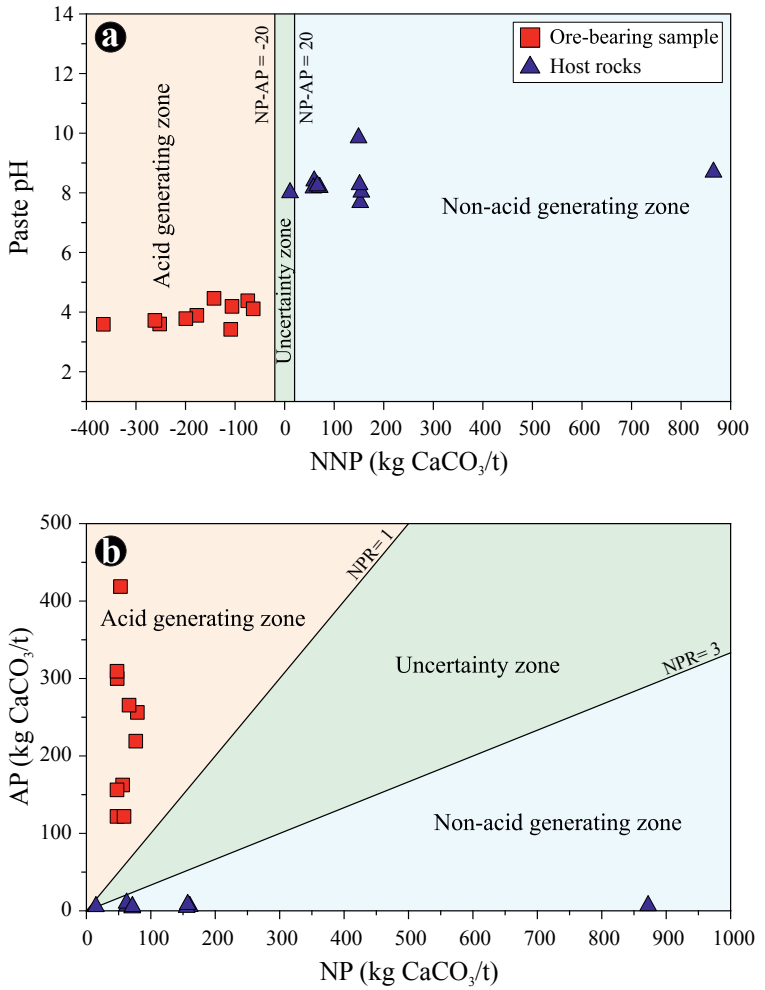

Figure 7. The ABA diagrams of studied rocks. **(a)** Classification of the samples according to Paste pH versus NNP (criteria used to interpret the results of ABA are according to Ferguson and Morin, 1991) and, **(b)** Classification of the samples in terms of AP and NP (Sobek et al., 1978; Brodie et al., 1991; Lapakko, 2002).

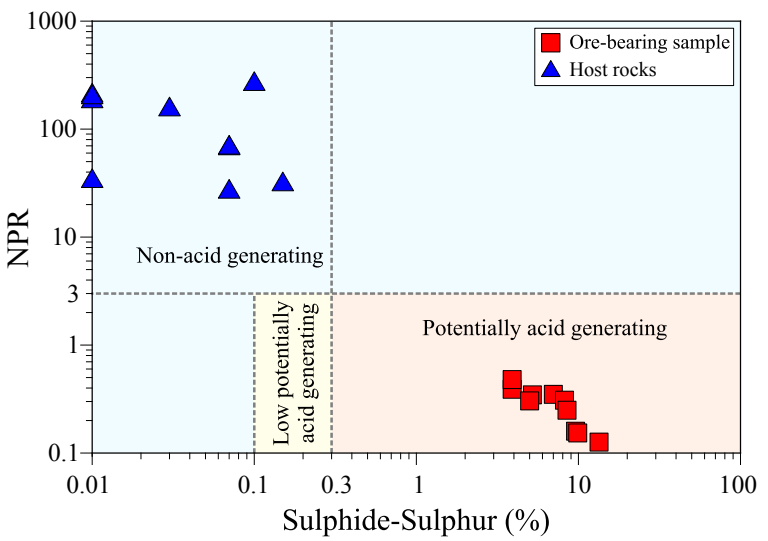

Figure 8. NPR vs Sulphide-Sulphur (%) diagram showing acid prediction zones and distribution of studied samples (criteria used to interpret the results are according to Sobek et al., 1978; Price et al., 1997).

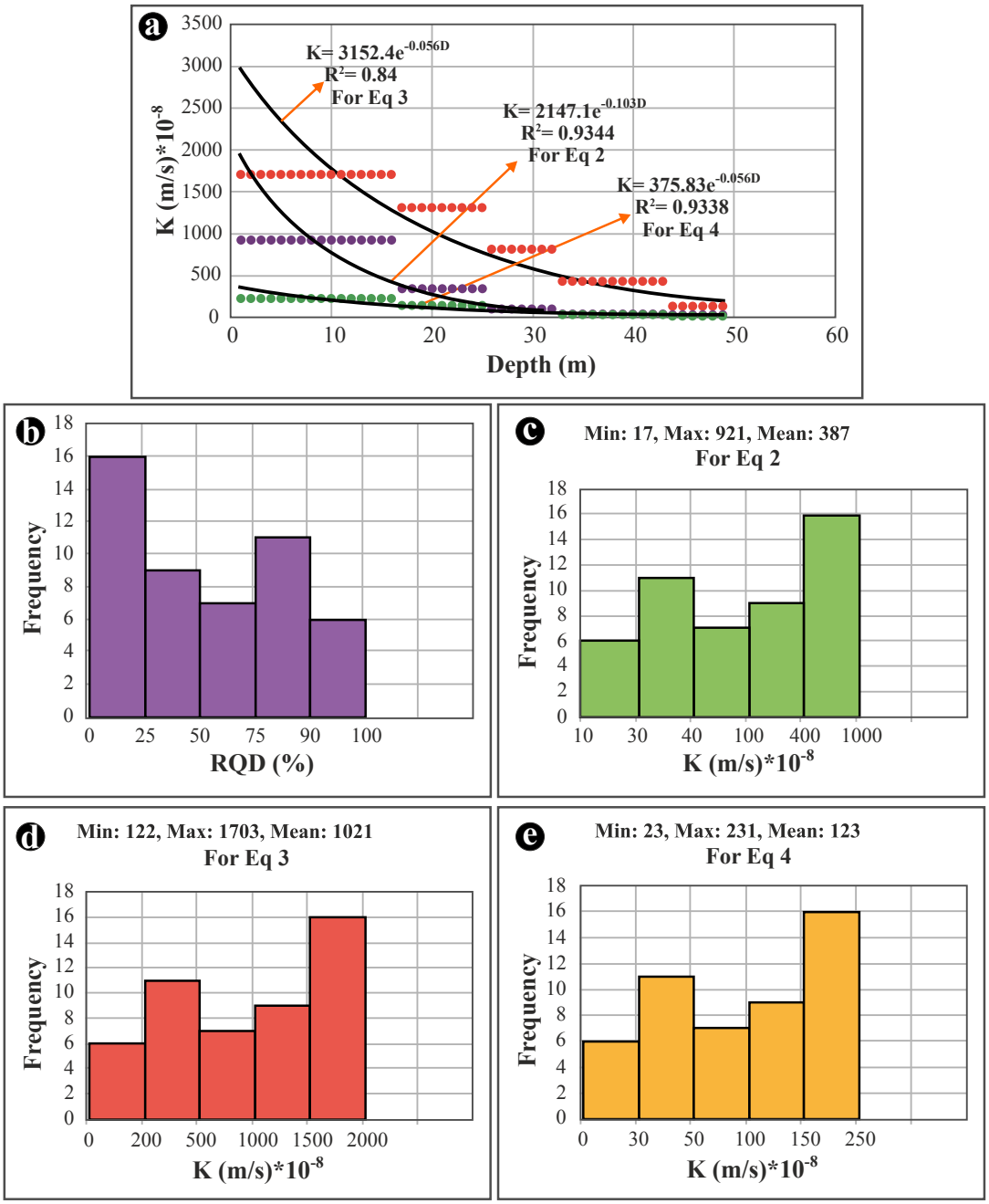

Figure 9. (a) Change in the depth of rock mass permeability in the stock area, **(b)** RQD (%) distribution histogram of wells BH-135, **(c-e)** Histogram distributions of permeability according to equation 2, 3 and 4.

In the study area, the seepage of the stockpile area was analyzed using the RS2 software (Rocscience, 2019). The Seepage behavior of the material in two-dimensional groundwater steady state FEA conditions was modeled using finite element groundwater seepage. The seepage analysis for the stockpile area was carried out using the using generalized Hoek-Brown failure criterion to investigate permeability. The rock mass environment was chosen as plastic and isotropic. A graded and six-node triangular finite element mesh was used in the stockpile area seepage model. For modeling, in addition, the discharge section plane was added to determine the steady-state volumetric flow rate that will occur in the rock mass. The vertical hydraulic conductivity value obtained as a result of the analysis with RS2 is 1.7×10^{-5} m/s in the stock area base rock (Figure 10). This indicates that the rock mass spreading in the stock area is of slightly permeability. Water leakage occurring in the discharge section (Figure

11) drawn at a depth of 5 m after the membrane coating applied at the floor of the stock area was determined as 1.34 × 10^{-17} m^3/s. These water leaks are very low since the rock mass has semipermeable character, and no contamination is expected in the groundwater in the rock mass.

5. Conclusions and suggestions

The results of the studies to determine the formation of potential AMD in the ore deposit and stockpile areas, and the remediation studies in case of a potential AMD development are summarized below.

The enrichment of Fe_2O_3 contents in both ore samples and host rocks is related to the mafic minerals and the alterations. On the one hand, the enrichment of Cr, Cu, Mn, and Zn is associated with mineral paragenesis and alterations such as hematitic and limonitic. Similarly, based on the contact leaching results, the high Fe, Cu, Zn, Cd, Co, and Ni concentrations in the samples are also associated with mineral paragenesis and alterations. The pH values in ore samples range from 3.27 to 4.05, indicating the acidic environment and class-IV water quality. According to base metal concentrations, especially high Cu values of 6.90–418.00 mg/L, the ore-bearing samples reflect potential acid rock/mine drainage characteristics. The NNP, NPR, and sulphide-sulphur values obtained in ore-bearing samples show that there is AMD formation potential in the region. Depending on selected static test results, the following studies are recommended against possible AMD formation and rock mass permeability.

The hydraulic conductivity value of basalt rock mass, which constitutes the basement rock of the stock field, was determined as slightly permeable as a result of the empirical equation. The geomembrane cover process to be applied at the stockpile area floor was modeled by seepage analysis using the finite element method, and the steady-state volumetric flow rate was determined as 1.34 × $10^{-17}$$m^3$/s. This value, determined for a depth of 5 m from the

Table 7 Permeability values for jointed rock masses (ISRM, 1981)

Rock Mass Description	Permeability Degree	Hydraulic Conductivity (K) (m/s)
Very closely spaced joints	Highly permeable	$1\text{-}10^{-2}$
Closely to moderately spaced	Medium permeable	$10^{-2}\text{-}10^{-5}$
Widely to very widely spaced	Slightly permeable	$10^{-5}\text{-}10^{-9}$
Unjointed, massive	Impermeable	$<10^{-9}$

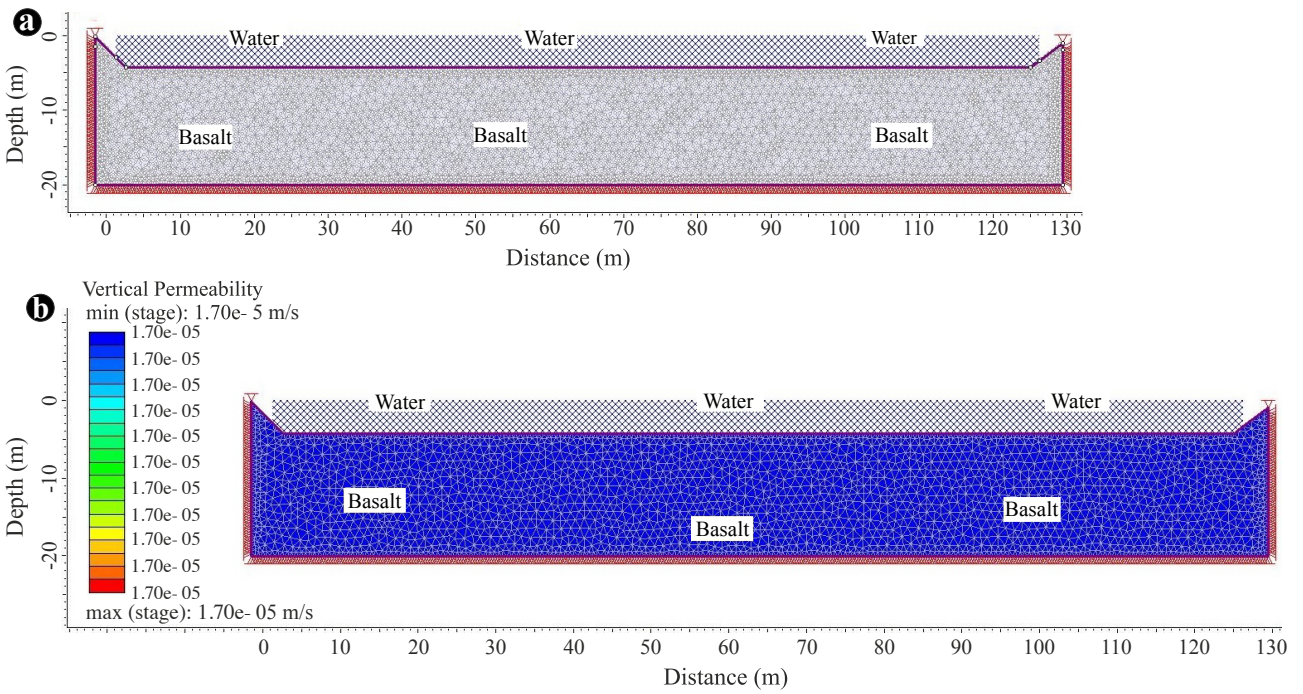

Figure 10. (a) Finite element network model, **(b)** Vertical permeability analysis in stockpile area.

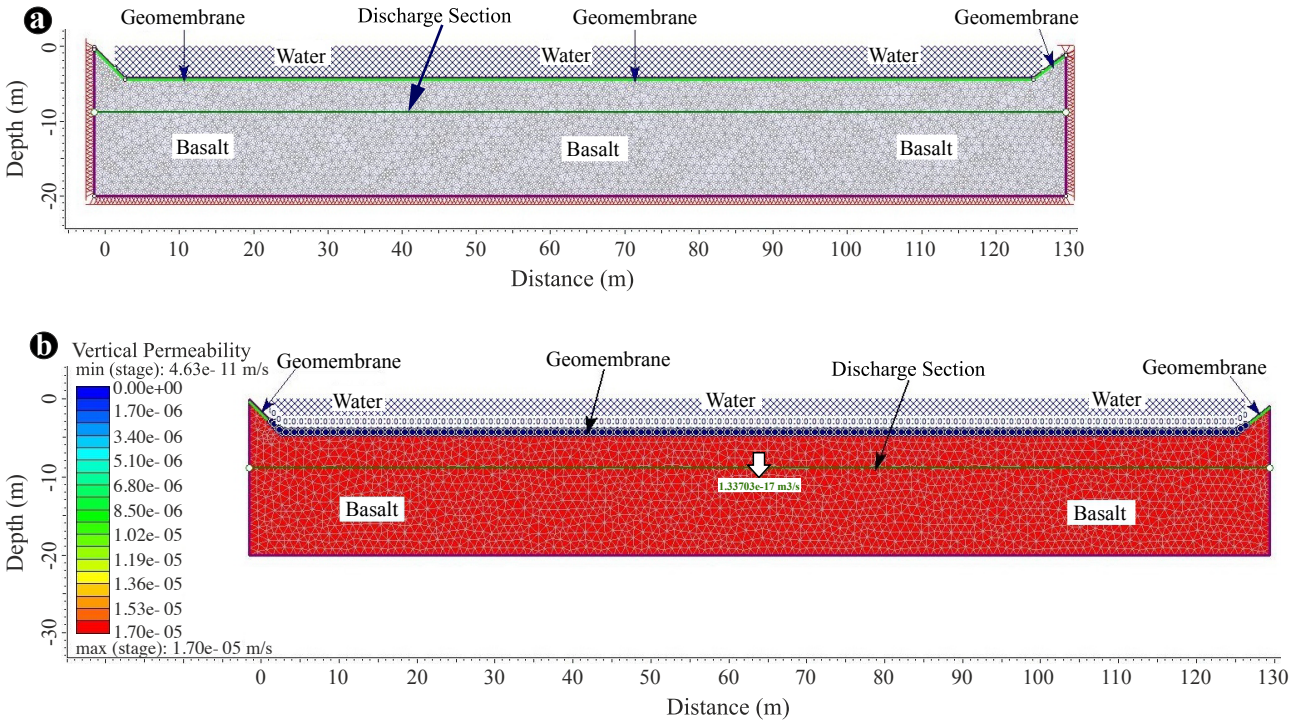

Figure 11. (a) Finite element network model after membrane coating in the stockpile area, **(b)** Vertical permeability analysis in stockpile area.

floor of the stock area, means that the membrane coating is useful and will prevent possible groundwater pollution.

Acknowledgments

We would like to thank the Esen Madencilik Sanayi Ticaret AŞ, who provided financial support to this study and helped to collect samples from the study area and analyze them. In addition, the authors would like to thank the handling editor and the anonymous reviewers, who evaluated the manuscript and made useful contributions to its content.

References

Adedokun TA, Abubakar A (2016). Relationship between Hydraulic Conductivity of Rock and Rock Quality Designation of Itisi Multi-Purpose Dam. International Journal on Recent and Innovation Trends in Computing and Communication, 4 (4): 126-135.

Akaryalı E, Gücer MA, Alemdag S (2018). Atık Barajı Rezervuarı ve Cevher Stok Alanlarında Asit Maden Drenajı (AMD) Oluşumunun Değerlendirilmesi: Gümüşhane Örneği. Doğal Afetler ve Çevre Dergisi, 4 (2): 192-209 (in Turkish with English abstract).

Akçil A, Koldaş S (2006). Acid Mine Drainage (AMD): Causes, Treatment and Case Studies. Journal of Cleaner Production 14 (12-13): 1139-1145.

Alemdag S (2015). Assessment of bearing capacity and permeability of foundation rocks at the Gumustas waste dam site, (NE Turkey) using empirical and numerical analysis. Arabian Journal of Geosciences 8: 1099-1110.

Alemdag S, Akaryalı E, Gücer MA (2020). Flotasyon Tesis Atıklarının Asit Üretme Potansiyeli ve Kirliliğin Önlenmesi, Gümüşhane, KD Türkiye. Yerbilimleri 41(1): 56-85 (in Turkish with English abstract).

Baba A, Kavdır Y, Deniz O (2004). The impact of an open waste disposal site on soil and groundwater pollution. International Journal of Environment and Pollution 22 (6): 676-687.

Balcı N, Demirel C (2018). Prediction of Acid Mine Drainage (AMD) and Metal Release Sources at the Küre Copper Mine Site, Kastamonu, NW Turkey. Mine Water and the Environment 37: 56-74.

BCAMDTF (British Columbia Acid Mine Drainage Task Force) (1989). Draft Acid Rock Drainage Technical Guide - Volume 1. Prepared by Steffen Robertson and Kirsten (SRK), Vancouver, BC.

Betrie GD, Sadiq R, Morin KA, Tesfamariam S (2015). Ecological risk assessment of acid rock drainage under uncertainty: The fugacity approach. Environmental Technology and Innovation 4: 240-247.

Blowes DW, Jambor JL (1990). The pore-water geochemistry and the mineralogy of the vadose zone of sulfide tailings, Waite amulet, Quebec, Canada. Applied Geochemistry 5: 327-346.

Boon M, Heijnen JJ (1998). Chemical oxidation kinetics of pyrite in bioleaching processes. Hydrometallurgy 48: 27-41.

Bouffard SC, Rivera-Vasquez BF, Dixon DG (2006). Leaching kinetics and stoichiometry of pyrite oxidation from a pyrite–marcasite concentrate in acid ferric sulfate media. Hydrometallurgy 84: 225-238.

Bouzahzah H, Benzaazoua M, Bussiere B, Plante B (2014). Prediction of Acid Mine Drainage: Importance of Mineralogy and the Test Protocols for Static and Kinetic Tests. Mine Water and the Environment 33: 54-65.

Bradham WS, Caruccio FT (1991). A comparative study of tailings analysis using acid/base accounting, cells, columns and Soxhlets. In: 2nd International Conference on the Abatement of Acidic Drainage, Montréal, CANMET, Ottawa, Canada, 1: 157-173.

Brady K, Hornberger R, Chisholm W, Sames G (2000). How geology affects mine drainage prediction. In: Kleinmann RLP (editor): Prediction of water quality at surface coal mines (pp. 8-35). West Virginia: The National Mine Land Reclamation Center.

Brodie MJ, Broughton LM, Robertson A (1991). A conceptual rock classification system for waste management and a laboratory method for ARD prediction from rock piles. In: Proceedings 2nd ICARD 3: 119-135.

Brunner B, Yu J-Y, Mielke RE, MacAskill JA, Madzunkov S et al. (2008). Different isotope and chemical patterns of pyrite oxidation related to lag and exponential growth phases of *Acidithiobacillus ferrooxidans* reveal a microbial growth strategy. Earth and Planetary Science Letters 270: 63-72.

Caraballo MA, Rötting TS, Macías F, Nieto JM, Ayora C (2009). Field multi-step limestone and MgO passive system to treat acid mine drainage with high metal concentrations. Applied Geochemistry 24: 2301-2311.

Caraballo MA, Macías F, Rötting TS, Nieto JM, Ayora C (2011). Long term remediation of highly polluted acid mine drainage: A sustainable approach to restore the environmental quality of the Odiel river basin. Environmental Pollution 159: 3613-3619.

Cidu R, Frau F (2009). Abandoned and active mining sites: From contamination to remediation. Journal of Geochemical Exploration 100 (2-3). doi: 10.1016/j.gexplo.2008.06.002.

Çimen O, Öztüfekçi Önal A, Akyol EA (2018). Assessment of pollution potential of the Hasangazi chromite pit (Tunceli, Turkey): implications for the natural environment. Environmental Earth Sciences 77: 199. doi: 10.1007/s12665-018-7391-9.

De Capitani L, Grieco G, Porro S, Ferrari E, Roccotiello E et al. (2014). Potentially toxic element contamination in waste rocks, soils and wild flora at the Roșia Montană mining area (Romania). Periodico di Mineralogia 83: 223-239.

Deere DU (1964). Technical description of rock cores for engineering purposes. Rock Mechanics and Engineering Geology 1 (1): 16-22.

Delibalta MS, Uzal N, Lermi A (2016). Acid Mine Drainage and Rehabilitation in Ilgın Lignite Mines Lakes. Niğde University Journal of Engineering Sciences 5 (1): 73-82.

Descostes M, Vitorge P, Beaucaire C (2004). Pyrite dissolution in acidic media. Geochimica et Cosmochimica Acta 68: 4559-4569.

Dold B (2017). Acid rock drainage prediction: A critical review. Journal of Geochemical Exploration 172: 120-132.

Dold B (2014). Evolution of acid mine drainage formation in sulphidic mine tailings. Minerals 4 (2): 621-641.

Dold B, Wade C, Fontboté L (2009). Water management for acid mine drainage control at the polymetallic Zn-Pb-(Ag-Bi-Cu) deposit Cerro de Pasco, Peru. Journal of Geochemical Exploration 100: 133-141.

EPA (US Environmental Protection Agency) (1994a). Innovative Methods of Managing Environmental Releases at Mine Sites, USEPA, Office of Solid Waste, Special Wastes Branch (Washington DC), April, OSW Doc. 530-R-94-012.

EPA (US Environmental Protection Agency) (1994b). Acid Mine Drainage Prediction, USEPA, Office of Solid Waste, Special Wastes Branch (Washington DC), December, EPA 530-R-94-036.

Farid AT, Rizwan M (2017). Prediction of in situ permeability for limestone rock using rock quality designation index. International Journal of Geotechnical and Geological Engineering 11 (10): 948-951.

Ferguson KD, Morin KA (1991). The prediction of acid rock drainage-lessons from the database. In: Proceedings of the 2nd ICARD, vol 1-4. Montréal, QC, Canada. pp 83-106.

Ficklin WH, Plumlee GS, Smith KS, McHugh JB (1992). Geochemical classification of mine drainages and natural drainages in mineralized areas. In: Kharaka YK, Maest AS (editors). Proceedings of water-rock interaction no 7. Balkema, Rotterdam. pp 381-384.

Frostad SR, Price WA, Bent H (2003). Operational NP determination-accounting for iron manganese carbonates and developing a site-specific fizz rating. In: Spiers G, Beckett P, Conroy H (editors). Mining and the environment, Sudbury 2003. Laurentian University, Sudbury. pp 231-237.

Gleisner M, Herbert RB, Kockum PCF (2006). Pyrite oxidation by Acidithiobacillus ferrooxidans at various concentrations of dissolved oxygen. Chemical Geology 225: 16-29.

Gray N (1997). Environmental impact and remediation of acid mine drainage: a management problem. Environmental Geology 30: 62-71.

Gurocak Z, Alemdag S (2012). Assessment of permeability and injection depth at the Atasu dam site (Turkey) based on experimental and numerical analyses. Bulletin of Engineering Geology and the Environment 71: 221-229.

Hoek E, Carranza-Torres CT, Corkum B (2002). Hoek-Brown failure criterion-2002 edition. In: Proceedings of the 5th North American Rock Mechanics Symposium; Toronto, Canada. pp. 267-273.

Holmes PR, Crundwell FK (2000). The kinetics of the oxidation of pyrite by ferric ions and dissolved oxygen: an electrochemical study. Geochimica et Cosmochimica Acta 64: 263-274.

Hossner LR, Brandt JE (1997). Acid/Base Account and Minesoils: A Review. In: Proceedings of 14th Annual Meeting of the ASSMR. America Society of Mining and Reclamation. pp 128-140.

ISRM (International Society for Rock Mechanics) (1981). ISRM Suggested Method: Rock Characterization, Testing and Monitoring. In: Brown, E.T. (editor). London, UK: Pergamon Press.

ISRM (International Society for Rock Mechanics) 2007. The complete ISRM suggested methods for rock characterization. In: Ulusay R, Kazan Hudson JA (editors). Testing and Monitoring. Ankara, Turkey: Offset Press. 628 p.

İmer A, Richards JP, Creaser RA (2013). Age and tectonomagmatic setting of the Eocene Çöpler–Kabataş magmatic complex and porphyry-epithermal Au deposit, East Central Anatolia, Turkey. Mineralium Deposita 48: 557-583.

İmer A, Richards JP, Muehlenbachs K (2016). Hydrothermal Evolution of the Çöpler Porphyry-Epithermal Au Deposit, Erzincan Province, Central Eastern Turkey. Economic Geology 111 (7): 1619-1658.

Jia Y, Tan Q, Sun H, Zhang Y, Gao H et al. (2018). Sulfide mineral dissolution microbes: Community structure and function inindustrial bioleaching heaps. Green Energy and Environment 4 (1): 29-37.

Kalyoncu Erguler G, Erguler ZA, Akcakoca H, Ucar A (2014). The effect of column dimensions and particle size on the results of kinetic column test used for acid mine drainage (AMD) prediction. Minerals Engineering 55: 18-29.

Kalyoncu Erguler G, Erguler ZA (2020). The evaluation of acid mine drainage by kinetic procedures and empirical models for field scale behaviour. Arabian Journal of Geosciences 13: 387.

Kanık M, Ersoy H (2019). Evaluation of the engineering geological investigation of the Ayvalı dam site (NE Turkey). Arabian Journal of Geosciences 12: 89. doi: 10.1007/s12517-019-4243-1

Karsli O, Chen B, Uysal I, Aydin F, Wijbrans JR et al. (2008). Elemental and Sr-Nd-Pb isotopic geochemistry of the most recent Quaternary volcanism in the Erzincan Basin, Eastern Turkey: framework for the evaluation of basalt-lower crust interaction. Lithos 106: 55-70.

Kayabasi A, Yesiloglu-Gultekin N, Gokceoglu C (2015). Use of non-linear prediction tools to assess rock mass permeability using various discontinuity parameters. Engineering Geology 185: 1-9.

Keskin M, Pearce JA, Kempton PD, Greenwood P (2006). Magma-crust interactions and magma plumbing in a postcollisional setting: Geochemical evidence from the Erzurum-Kars volcanic plateau, eastern Turkey. Geological Society of America Special Paper 409: 475-505.

Khoeurn K, Sakaguchi A, Tomiyama S, Igarashi T (2019). Long-term acid generation and heavy metal leaching from the tailings of Shimokawa mine, Hokkaido, Japan: Column study under natural condition. Journal of Geochemical Exploration 201: 1-12.

Köppen W (1918). Klassification der Klimate nach Temperatur, Niederschlag and Jahreslauf. Petermanns Geographische Mitteilungen 64: 193-248.

Lapakko KA (2002). Metal mine rock and waste characterization tools: an overview. Mining, Minerals and Sustainable Development 67: 1-31.

Lawrence RW, Marchant PB (1991). Acid Rock Drainage Prediction Manual. Report CANMET, MEND Project 1.16.1b, Canada.

Lawrence RW, Poling GW, Ritcey GM, Marchant PB (1989). Assessment of predictive methods for the determination of AMD potential in mine tailings and waste rock, tailings and effluent management. Pergamon Press, New York. pp. 317-331.

Lawrence RW, Scheske M (1997). A method to calculate the neutralization potential of mining wastes. Environmental Geology 32: 100-106.

Lawrence RW, Wang Y (1996). Determination of neutralizing potential for acid rock drainage prediction. MEND/NEDEM report 1.16.3, Canadian Centre for Mineral and Energy Technology, Ottawa, ON, Canada.

Liu C, Jia Y, Sun H, Tan Q, Niu X et al. (2017). Limited role of sessile acidophiles in pyrite oxidation below redox potential of 650 mV. Scientific Reports 7 (1): 5032. doi: 10.1038/s41598-017-04420-2.

Lottermoser BG (2010). Mine Wastes: Characterization, Treatment and Environmental Impacts, 3rd ed. Heidelberg, Berlin: Springer.

Ma Y, Lin C (2013). Microbial oxidation of Fe and pyrite exposed to flux of micromolar H_2O_2 in acidic media. Scientific Reports 3: 1350-1352.

MEND (Mine Environment Neutral Drainage) (2009). Prediction manual for drainage chemistry from sulphidic geologic materials. In: CANMET-Mining and Mineral Sciences Laboratories, Smithers, British Columbia, Canada. MEND report 1.20.1, 579 p.

Michaud ML, Plante B, Bussière B, Benzaazoua M, Leroux J (2017). Development of a modified kinetic test using EDTA and citric acid for the prediction of contaminated neutral drainage. Journal of Geochemical Exploration 181: 58-68.

Morin KA, Hutt NM (2001). Environmental geochemistry of minesite drainage: practical theory and case studies. MDAG Publishing, Vancouver.

Nordstrom DK (2009). Acid rock drainage and climate change. Journal of Geochemical Exploration 100: 97-104.

Okay AI, Tüysüz O (1999). Tethyan sutures of northern Turkey. The Mediterranean basin: Tertiary extension within the Alpine orogeny. Geological Society, London, Special Publications 156: 475-515.

Parbhakar-Fox A, Lottermoser B, Bradshaw D (2013). Evaluating waste rock mineralogy and microtexture during kinetic testing for improved acid rock drainage prediction. Minerals Engineering 52:111-124.

Park I, Tabelin CB, Jeon S, Li X, Seno K, Ito M, Hiroyoshi N (2019). A review of recent strategies for acid mine drainage prevention and mine tailings recycling. Chemosphere 219: 588-606.

Parlak O, Çolakoğlu A, Dönmez C, Sayak H, Yıldırım N et al. (2013). Geochemistry and tectonic significance of ophiolites along the Ankara–Erzincan Suture Zone in northeastern Anatolia. In: Robertson AHF, Parlak O, Ünlügenç UC (editors). Geological Society, London, Special Publications 372: 75-105.

Plumlee GS, Smith KS, Ficklin WH, Briggs PH (1992). Geological and geochemical controls on the composition of mine drainages and natural drainages in mineralized areas. In: Proceedings, 7th International Water-Rock Interaction Conference, Park City, Utah. pp. 419-422.

Plumlee GS, Smith KS, Montour MR, Ficklin WH, Mosier EL (1999). Geologic controls on the composition of natural waters and mine waters draining diverse mineral-deposit types. In: Filipek LH, Plumlee GS (editors). The environmental geochemistry of mineral deposits. Part B: case studies and research topics, vol 6B. Society of Economic Geologists, Littleton. pp. 373-432 (Reviews in Economic Geology).

Price WA, Errington J, Koyanagi V (1997). Guidelines for the prediction of acid rock drainage and metal leaching for mines in British Columbia: part I. General procedures and information requirements. In: Proceedings, 4th ICARD, Natural Resources Canada, Ottawa 1: 1-14.

Price WA (2003). Challenges posed by metal leaching and acid rock drainage, and approaches used to address them. In: Jambor JL, Blowes DW, Ritchie AIM (editors). Environmental aspects of mine wastes. Mineralogical Association of Canada, Short Course Series 31: 15-30.

Rastegarnia A, Lashkaripour GR, Ghafoori M, Farrokhad SS (2019). Assessment of the engineering geological characteristics of the Bazoft dam site, SW Iran. Quarterly Journal of Engineering Geology and Hydrogeology 52: 360-374.

RG (Resmi Gazete/Turkish Official Gazette) 28483 (2012). Regulation on Surface Water Quality Management, the Turkish Standards, Ankara (revision: RG-15/4/2015-29327).

Rocscience (2019). RS2 10.012 2D Geotechnical Finite Element Analysis, Geomech Software and Res. Rocsci, Toronto.

Sapsford DJ, Bowell RJ, Dey M, Williams KP (2009). Humidity cell tests for the prediction of acid rock drainage. Minerals Engineering 22 (1): 25-36.Siddharth S, Jamal A, Dhar BB, Shukla R (2002). Acid-Base Accounting: A Geochemical Tool for Management of Acid Drainage in Coal Mines. Mine Water and the Environment 21: 106-110.

Singer PC, Stumm W (1970). Acidic Mine Drainage: The rate-determining step. Science 167: 1121-1123.

Skousen J, Perry E, Leavitt B, Sames G, Chisholm W, Cecil CB, Hammack R (2000a). Static tests for coal mining acid mine drainage prediction in the eastern U.S. In: Kleinmann RLP (editor): Prediction of water quality at surface coal mines (pp. 73-98). West Virginia: The National Mine Land Reclamation Center.

Skousen JG, Sexstone A, Ziemkiewicz PF (2000b). Acid mine drainage control and treatment. In: Hartfield JL, Volenec JG, Dick WA (editors): Reclamation of drastically disturbed lands. American Society of Agronomy and American Society for Surface Mining and Reclamation. Agronomy 41: 131-169.

Skousen JG, Sencindiver JC, Smith RM (1987). A Review of Procedures for Surface Mining and Reclamation in Areas with Acid-Producing Materials. EWRC 871, West Virginia University, Morgantown, WV, 40 pp.

Smith RM, Sobek AA, Arkle T, Sencindiver JC, Freeman JR (1976). Extensive overburden potentials for soil and water quality. EPA-600/2-76-184. USEPA, Cincinnati, OH.

Sobek AA, Schuller WA, Freeman JR, Smith RM (1978). Field and laboratory methods applicable to overburdens and minesoils. EPA-600/2-78-054. US Govt Printing Office, Washington, DC.

Soregaroli BA, Lawrence RW (1998). Update on waste characterisation studies. In: Proceedings mine design, operations and closure conference, Polson, MT, USA.

Şanlıyüksel Yücel D, Baba A (2013). Geochemical Characterization of Acid Mine Lakes in Northwest Turkey and Their Effect on the Environment. Archives of Environmental Contamination and Toxicology 64: 357-376.

Şanlıyüksel Yücel D, Baba A (2016). Prediction of acid mine drainage generation potential of various lithologies using static tests: Etili coal mine (NW Turkey) as a case study. Environmental Monitoring and Assessment 188: 473, doi: 10.1007/s10661-016-5462-5.

Şanlıyüksel Yücel D, Balcı N, Baba A (2016). Generation of acid mine lakes associated with abandoned coal mines in NW Turkey. Archives of Environmental Contamination and Toxicology 70 (4): 757-782.

Şengör AMC, Özeren S, Genç T, Zor E (2003). East Anatolian high plateau as a mantle-supported, north-south shortened domal structure. Geophysical Research Letters 30 (24): 8045.

Tayfur G, Tanji KK, Baba A (2010). Two-dimensional finite elements model for selenium transport in saturated and unsaturated zones. Environmental Monitoring and Assessment 169: 509-518.

Tosun Yİ (2017). Thickener Water Neutralization by Mid-Bottom and Fly Ash of Thermal Power Plants and CO_2: Organic Humate Mud of AMD Treatment for Remediation of Agricultural Fields. In: Akinyemi SA, Gitari MW (editors). Coal Fly Ash Beneficiation - Treatment of Acid Mine Drainage with Coal Fly Ash. IntechOpen, pp: 141-169, doi: 10.5772/intechopen.69927.

US Bureau of Reclamation (1974). Field permeability tests (well permeameter method). Test designation #E-19, 2nd ed. earth manual.

Verburg R, Bezuidenhout N, Chatwin T, Ferguson K (2009). The global acid rock drainage guide (GARD guide). Mine Water and the Environment 28: 305-310.

Yaroshevsky AA (2006). Abundances of chemical elements in the Earth's crust. Geochemistry International 44 (1): 54-62.

Yolcubal I, Demiray AD, Çiftçi E (2017). Assessment of acid mine drainage potential of flotation slurry from a tailing dam in a copper mine, Murgul, Northeastern Turkey. Environmental Earth Sciences 76 (100): 1-10, doi: 10.1007/s12665-017-6423-1.

Yolcubal I, Demiray AD, Çiftçi E, Sanğu E (2016). Environmental impact of mining activities on surface water and sediment qualities around Murgul copper mine, Northeastern Turkey. Environmental Earth Sciences 75 (1415): 1-25, doi: 10.1007/s12665-016-6224-y.